Ceramics International 51 (2025) 7229–7235

Contents lists available at ScienceDirect

Ceramics International

journal homepage: www.elsevier.com/locate/ceramint

# Enhanced piezoelectric performance in lead-free piezoceramics of (1–$x$) $Bi_{0.5}Na_{0.5}TiO_3$-$xBa(Sc_{0.5}Nb_{0.5})O_3$

Weihao Li [a,b], Zhao Pan [b,*], Mengqi Ye [b], Jin Liu [b], Maocai Pi [b], Jie Zhang [b], Xubin Ye [b], Xiao Wang [b], Nianpeng Lu [b], Laijun Liu [c], Enxiu Wu [a,**], Youwen Long [b,d,e,***]

[a] School of Precision Instruments and Opto-electronics Engineering, Tianjin University, No. 92 Weijin Road, Tianjin, 300072, China
[b] Beijing National Laboratory for Condensed Matter Physics, Institute of Physics, Chinese Academy of Sciences, Beijing, 100190, China
[c] Guangxi Key Lab of Optical and Electronic Functional Materials and Devices, College of Materials Science and Engineering, Guilin University of Technology, Guilin, 541004, China
[d] School of Physical Sciences, University of Chinese Academy of Sciences, Beijing, 100049, China
[e] Songshan Lake Materials Laboratory, Dongguan, Guangdong, 523808, China

ARTICLE INFO

Handling Editor: P. Vincenzini

ABSTRACT

A novel lead-free piezoelectric system, (1-$x$)$Bi_{0.5}Na_{0.5}TiO_3$-$xBa(Sc_{0.5}Nb_{0.5})O_3$ ((1-$x$)BNT-$x$BSN), was developed using a conventional solid-state synthesis method. The effect of $Ba(Sc_{0.5}Nb_{0.5})O_3$ substitution on the crystal structure, microstructure, and electrical properties of $Bi_{0.5}Na_{0.5}TiO_3$ were studied systematically. All studied compositions display a pure perovskite phase. Note that the introduction of $Ba(Sc_{0.5}Nb_{0.5})O_3$ significantly reduces the coercive field of $Bi_{0.5}Na_{0.5}TiO_3$. The 0.96BNT-0.04BSN compound exhibits superior piezoelectric properties, with an enhanced piezoelectric coefficient $d_{33}$ of 110 pC/N, nearly double that of the original $Bi_{0.5}Na_{0.5}TiO_3$. The P($E$) loops and S($E$) curves of 0.96BNT-0.04BSN demonstrate a ferroelectric to antiferroelectric phase transition at temperatures exceeding 100 °C. In addition, the 0.96BNT-0.04BSN ceramic also shows a moderate high phase transition temperature of 266 °C. The present study provides a new high piezoelectric performance lead-free ceramic based on $Bi_{0.5}Na_{0.5}TiO_3$, which could trigger the interesting in the studies on BNT-Ba($Me$)$O_3$ based Pb-free piezoelectric materials for high piezoelectric performance lead-free materials.

## 1. Introduction

Piezoelectric ceramics are capable of direct and reversible conversion of electrical energy into mechanical energy, which is widely used in sensors, high-frequency filters, and ultrasonic transducers [1–3]. Lead-based piezoelectric ceramics, particularly $PbTi_{1-x}Zr_xO_3$ (PZT), dominate the commercial market due to their superior piezoelectric properties at the morphotropic phase boundary (MPB) [4]. However, lead is toxic to environment and human health. Therefore, to ensure sustainable development for both humanity and the environment, it is imperative to investigate lead-free piezoelectric ceramics as alternatives to the existing PZT [5–7].

Over recent decades, various potential lead-free piezoelectric ceramics have been developed, including $Bi_{0.5}Na_{0.5}TiO_3$ (BNT), $Bi_{0.5}K_{0.5}TiO_3$ (BKT), $K_{0.5}Na_{0.5}NbO_3$ (NN), $BaTiO_3$ (BT), and their derivatives [8–16]. BNT is regarded as a promising candidate due to its significant remanent polarization ($P_r$ = 38 μC/cm$^2$) [17,18]. BNT is a room-temperature perovskite ferroelectric with rhombohedral symmetry (space group $R3c$). It undergoes a ferroelectric-to-paraelectric phase transition around at 320 °C, and a noticeable ferroelectric-to-antiferroelectric transition occurs at ~200 °C [19]. However, pure BNT exhibits a significant coercive field ($E_C$ = 7.3 kV/mm) and elevated conductivity, complicating the poling process [20]. Consequently, pure BNT ceramic typically demonstrates weak piezoelectric properties, characterized by a low piezoelectric coefficient of $d_{33}$ = 58 pC/N [8]. Various efforts have been undertaken to enhance the piezoelectric properties of BNT by creating BNT-based solid solutions, including BNT-$Bi(Zn_{1/2}Ti_{1/2})O_3$, BNT-$Bi(Mg_{1/2}Ti_{1/2})O_3$, and BNT-$Bi_{0.5}K_{0.5}TiO_3$ [21–23].

Following the report of exceptional piezoelectric properties in (1-$x$)

* Corresponding author.
** Corresponding author.
*** Corresponding author. Beijing National Laboratory for Condensed Matter Physics, Institute of Physics, Chinese Academy of Sciences, Beijing, 100190, China.
*E-mail addresses:* zhaopan@iphy.ac.cn (Z. Pan), enxiuwu@tju.edu.cn (E. Wu), ywlong@iphy.ac.cn (Y. Long).

https://doi.org/10.1016/j.ceramint.2024.12.157
Received 14 October 2024; Received in revised form 20 November 2024; Accepted 10 December 2024
Available online 10 December 2024

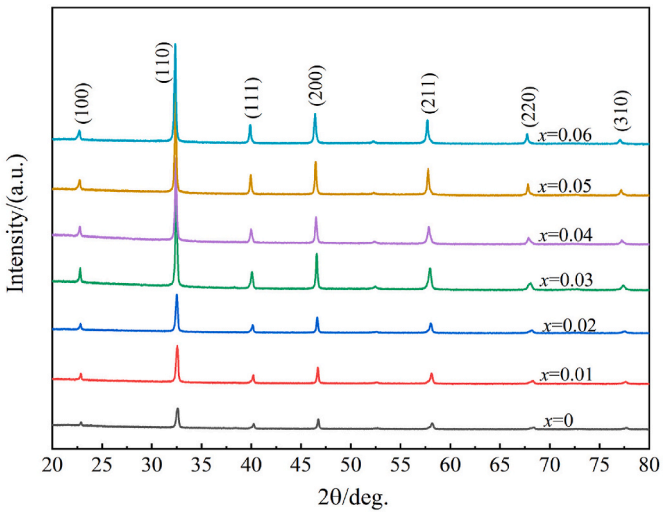


**Fig. 1.** X-ray diffraction patterns of the (1-*x*)BNT-*x*BSN (*x* = 0.0–0.06) compounds.

BNT-*x*$BaTiO_3$ near the MPB (*x* = 0.06), several high-performance lead-free ceramics were discovered within the BNT-Ba*Me*$O_3$ system, where *Me* represents a single or mixed cation(s) with an average valence of +4 [19,24–26]. Indeed, large $d_{33}$ values were observed in (1-*x*)BNT-*x*Ba($Al_{0.5}Nb_{0.5}$)$O_3$ and our recently reported (1-*x*)BNT-*x*Ba($Ni_{1/3}Nb_{2/3}$)$O_3$ systems [27,28]. It is therefore proposed that the introduction of $Nb^{5+}$ could improve the piezoelectric properties of BNT [29]. $Nb^{5+}$ has been shown to enhance domain switching and improve the piezoelectric properties of traditional PZT ceramics by 'softening' them [30]. On the other hand, both large $d_{33}$ and high $T_C$ values were observed in the MPB of *x*$BiScO_3$-(1-*x*)$PbTiO_3$ (*x* = 0.36) [31]. It is considered that $Sc^{3+}$ can also benefit the piezoelectric properties. We therefore developed a novel binary lead-free piezoelectric system of (1-*x*)$Bi_{0.5}Na_{0.5}TiO_3$-*x*Ba($Sc_{0.5}Nb_{0.5}$)$O_3$. The crystal structure, microstructure, and piezoelectric, ferroelectric, and dielectric properties were systematically studied.

## 2. Experimental procedure

Perovskite piezoelectric ceramics of (1-*x*)$Bi_{0.5}Na_{0.5}TiO_3$-*x*Ba($Sc_{0.5}Nb_{0.5}$)$O_3$ (abbreviated as (1-*x*)BNT-*x*BSN) with *x* ranging from 0.0 to 0.06 were synthesized using the conventional solid-state method. $Bi_2O_3$ (99.99 %), $Na_2CO_3$ (99.8 %), $TiO_2$ (99.9 %), $BaCO_3$ (99.95 %), $Sc_2O_3$ (99.99 %), and $Nb_2O_5$ (99.9 %) were measured according to the stoichiometric formula. The starting materials were thoroughly mixed using hand milling in an agate mortor, ensuring the powders were as homogeneous as possible. The mixed powders were calcined at 850 °C for 3 h, followed by re-milling and pressing into pellets with an 8 mm diameter and 1 mm thickness. The pellets underwent sintering in a covered alumina crucible at 1150 °C for 2 h, with a heating and cooling rate of 5 °C per minute. To minimize the loss of Bi and Na owing to the volatility during the sintering process, the samples were embedded by the calcined powders.

The crystal structure of the investigated samples was identified by X-ray powder diffractometer (XRD, X'Pert PRO, Huber, Germany) using a CuKα radiation at 40 kV and 40 mA (λ = 1.5406 Å). Surface morphology of the ceramics was examined using a HITACHI SU8200 scanning electron microscope (SEM). All ceramics were polished to approximately 0.6 mm thickness for electrical measurements. Then, the polished pellets were uniformly sputtered with gold electrodes on both sides using the magnetron ion sputtering instrument. An aixACCT TF Analyzer 1000 ferroelectricity analyzer (Aachen, Germany) equipped with a Sios Mi-60 laser was employed to measure electric field-induced polarization *P*(*E*) and longitudinal strain *S*(*E*) curves in a silicone oil bath using a 1 Hz triangular waveform at room temperature. Piezoelectric measurements involved poling all samples in a silicone oil bath at room temperature with a DC electric field of 8 kV/mm for 5 min. The piezoelectric coefficient ($d_{33}$) of each poled sample was measured with a $d_{33}$ m (ZJ-3, Chinese Academy of Acoustics, Beijing, China) after 24 h of aging. Thermal depoling measurements of the piezoelectric properties were conducted by attaching Ag electrodes at different temperatures for 30 min. The dielectric constant ($\varepsilon_r$) and dielectric loss (tan$\delta$) were analyzed across varying frequencies and temperatures using an HP4294A impedance analyzer (Hewlett-Packard, Palo Alto, CA).

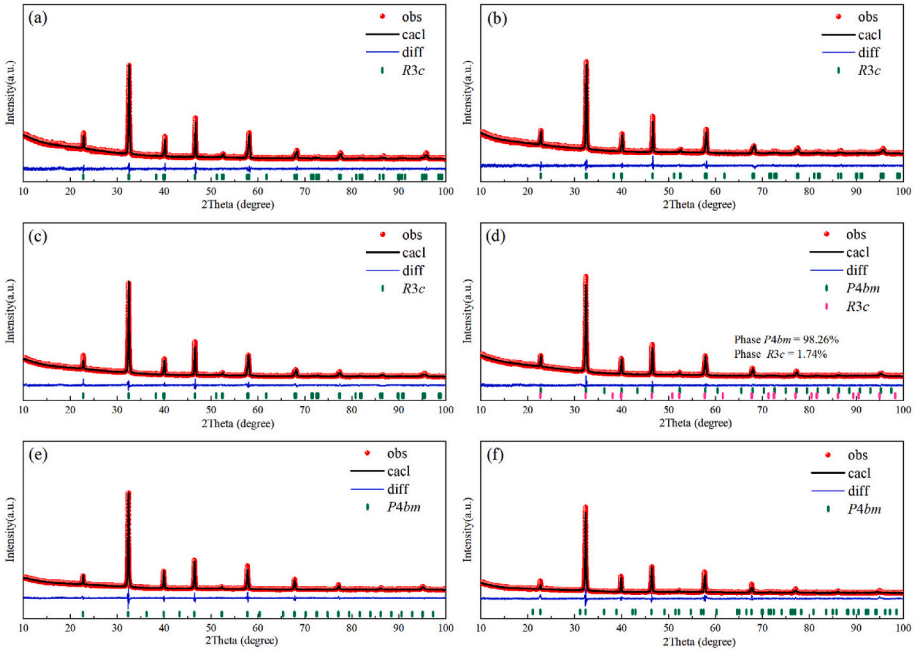


**Fig. 2.** Rietveld refinement results of (1-*x*)BNT-*x*BSN ceramics (a) *x* = 0.01, (b) *x* = 0.02, (c) *x* = 0.03, (d) *x* = 0.04, (e) *x* = 0.05, and (f) *x* = 0.06.

**Table 1**
Details of Rietveld refnement results of XRD patterns of the (1-*x*)BNT-*x*BSN ceramics.

| Sample | Space group | Atom | *x* | *y* | *z* | *U* | Cell (Å) | *R* (%) |
|---|---|---|---|---|---|---|---|---|
| $x = 0.01$ | *R3c* | Bi | 0 | 0 | 0.2734 | 0.0001 | $a = 5.479$ | $R_{wp} = 3.28$ |
| | | Na | 0 | 0 | 0.2487 | 0.0534 | $c = 13.520$ | $R_p = 2.49$ |
| | | Ba | 0 | 0 | 0.2734 | 0.0001 | | |
| | | Ti/Sc/Nb | 0 | 0 | 0.0094 | 0.0033 | | |
| | | O | 0.1130 | 0.3138 | 0.0732 | 0.0551 | | |
| $x = 0.02$ | *R3c* | Bi | 0 | 0 | 0.2349 | 0.0086 | $a = 5.489$ | $R_{wp} = 3.61$ |
| | | Na | 0 | 0 | 0.2349 | 0.0086 | $c = 13.532$ | $R_p = 2.65$ |
| | | Ba | 0 | 0 | 0.2349 | 0.0086 | | |
| | | Ti/Sc/Nb | 0 | 0 | −0.0092 | 0.0018 | | |
| | | O | 0.1130 | 0.3138 | 0.0773 | 0.0212 | | |
| $x = 0.03$ | *R3c* | Bi | 0 | 0 | 0.2714 | 0.0100 | $a = 5.500$ | $R_{wp} = 3.23$ |
| | | Na | 0 | 0 | 0.2487 | 0.0530 | $c = 13.574$ | $R_p = 2.30$ |
| | | Ba | 0 | 0 | 0.2714 | 0.0100 | | |
| | | Ti/Sc/Nb | 0 | 0 | 0.0094 | 0.0030 | | |
| | | O | 0.1130 | 0.3138 | 0.0732 | 0.0550 | | |
| $x = 0.04$ | *R3c* | Bi | 0 | 0 | 0.2345 | 0.0075 | $a = 5.530$ | $R_{wp} = 2.58$ |
| | | Na | 0 | 0 | 0.2345 | 0.0075 | $c = 13.539$ | $R_p = 2.00$ |
| | | Ba | 0 | 0 | 0.2345 | 0.0075 | | |
| | | Ti/Sc/Nb | 0 | 0 | −0.0120 | 0.0052 | | |
| | | O | 0.1130 | 0.3138 | 0.0752 | 0.0101 | | |
| | *P4bm* | Bi | 0 | 0.5 | 0.5358 | 0.0531 | $a = 5.517$ | |
| | | Na | 0 | 0.5 | 0.4795 | 0.0531 | $c = 3.902$ | |
| | | Ba | 0 | 0 | 0.4795 | 0.0531 | | |
| | | Ti/Sc/Nb | 0 | 0 | 0.0062 | 0.0030 | | |
| | | O1 | 0 | 0 | 0.5203 | 0.0448 | | |
| | | O2 | 0.2624 | 0.2376 | 0.0175 | 0.0289 | | |
| $x = 0.05$ | *P4bm* | Bi | 0 | 0.5 | 0.5153 | 0.0575 | $a = 5.524$ | $R_{wp} = 3.68$ |
| | | Na | 0 | 0.5 | 0.5153 | 0.0575 | $c = 3.905$ | $R_p = 2.56$ |
| | | Ba | 0 | 0 | 0.5153 | 0.0575 | | |
| | | Ti/Sc/Nb | 0 | 0 | −0.0138 | 0.0004 | | |
| | | O1 | 0 | 0 | 0.4859 | 0.0699 | | |
| | | O2 | 0.2700 | 0.2300 | 0.0477 | 0.0304 | | |
| $x = 0.06$ | *P4bm* | Bi | 0 | 0.5 | 0.5267 | 0.0377 | $a = 5.531$ | $R_{wp} = 4.23$ |
| | | Na | 0 | 0.5 | 0.5267 | 0.0377 | $c = 4.208$ | $R_p = 2.80$ |
| | | Ba | 0 | 0 | 0.5267 | 0.0377 | | |
| | | Ti/Sc/Nb | 0 | 0 | −0.0428 | 0.0251 | | |
| | | O1 | 0 | 0 | 0.3525 | 0.0344 | | |
| | | O2 | 0.2627 | 0.2373 | −0.0268 | 0.0581 | | |

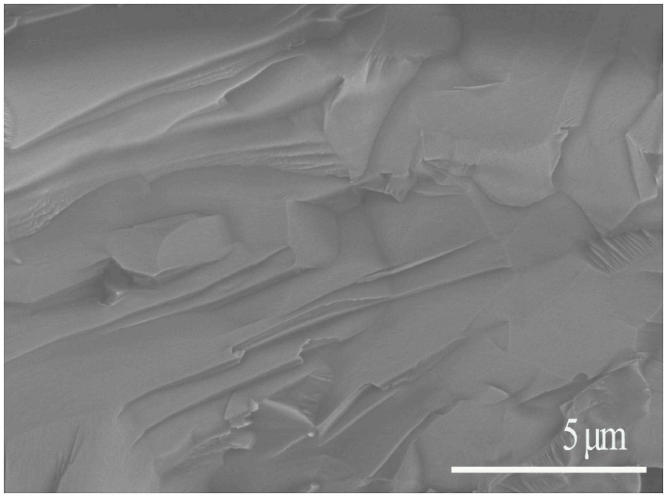


**Fig. 3.** SEM image of the 0.96BNT-0.04BSN ceramics.

## 3. Results and discussion

The XRD patterns were used to study the effect of BSN substation on the phase structure of BNT. As shown in Fig. 1, pure perovskite structure can be observed for all investigated samples, without any noticeable impurities. Note that the (200) peak around at $2\theta = 40$ gradually shifts to a lower $2\theta$ angle with increasing BSN content ($x$), indicating the lattice expansion. This may be attributed to the larger ionic radius of $Ba^{2+}$ (1.35 Å) compared to $Bi^{3+}$ (1.03 Å) and $Na^{+}$ (0.98 Å) at the *A*-site [32]. It therefore can be concluded that the BSN can be well incorporated into BNT matrix and lead to the lattice expansion.

The impact of BSN on BNT's phase structure was analyzed by refining XRD data for all samples using GSAS software [33], with results presented in Fig. 2.The details of the refined parameters are listed in Table 1. As can be seen, samples for $x \leq 0.03$ can be well refined by using the same rhombohedral symmetry to the pristine BNT (Fig. 2(a–c). Notably, with BSN content increasing to $x = 0.04$, a mixed *P4bm* and *R3c* phases coexist (Fig. 2(d)), indicating the so-called MPB could be located around at $x = 0.04$. For further increasing the BSN content, such as $x = 0.05$ and $x = 0.06$ (Fig. 2(e and f)), the samples were transformed into the single *P4bm* phase. The findings indicate that incorporating BSN into BNT triggers a phase transition from rhombohedral *R3c* to tetragonal *P4bm*, with both *R3c* and *P4bm* phases coexisting at $x = 0.04$.

Fig. 3 shows the SEM micrograph of selected BSN doped BNT ceramics with $x = 0.04$. As can be seen, the ceramic shows a dense and homogeneous microstructure. This suggests that the BNT-BSN ceramics were densely sintered.

Fig. 4 illustrates the room temperature evolution of polarization *P*(*E*) loops and bipolar strain *S*(*E*) curves as a function of the electric field for (1-*x*)BNT-*x*BSN ceramics with *x* values of 0.02, 0.04, and 0.05, near the MPB composition. Fig. 4(a) shows that all samples exhibit well saturated P(*E*) hysteresis loops, indicating typical ferroelectrics. Notably, *P*(*E*)

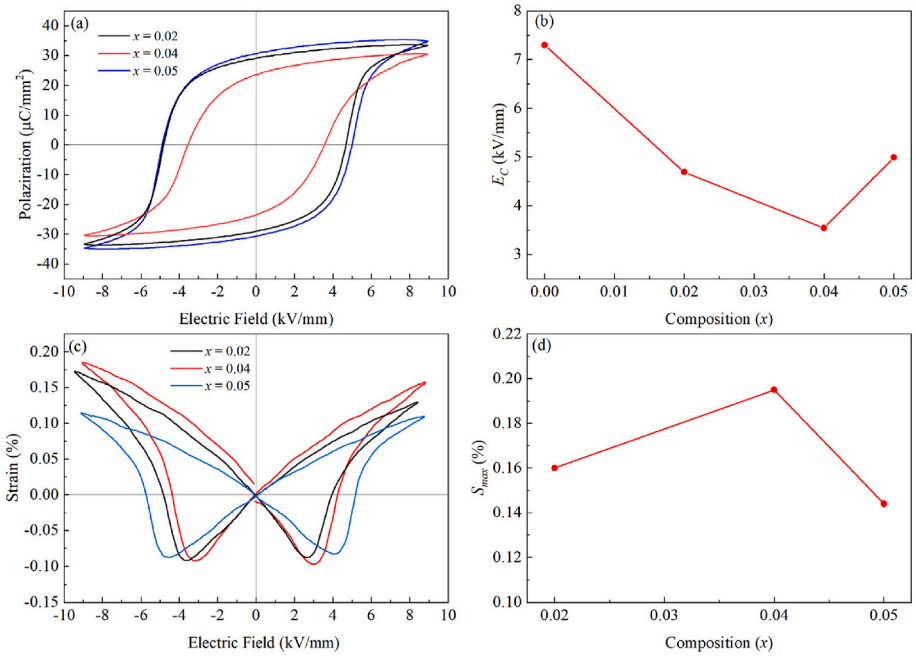


**Fig. 4.** (a) $P(E)$ hysteresis loops, (b) $E_C$, (c) bipolar $S(E)$ curves, and (d) $S_{max}$ of the (1-$x$)BNT-$x$BSN ceramics ($x$ = 0.02, 0.04, and 0.05).

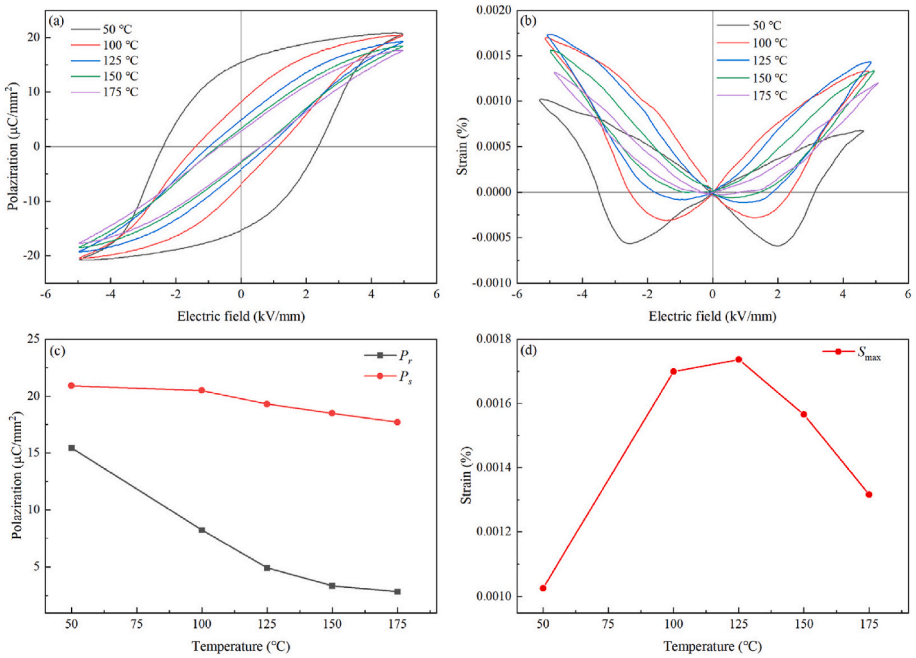


**Fig. 5.** (a) $P(E)$ ferroelectric loops, (b) bipolar $S(E)$ curves, (c) $P_S$ and $P_r$, and (d) the maximum strain for the 0.96BNT-0.04BSN ceramics as a function of temperature.

loops in the (1-$x$)BNT-$x$BSN system remain unconstricted even at a high BSN substitution level of $x$ = 0.05, indicating the sample retains its ferroelectric order (FE). This phenomenon is much different from the previously reported BNT-based systems, in which constrained $P(E)$ loops were usually observed for substitution contents beyond the MPB compositions. As can be seen, the introduction of BSN significantly reduces the coercive field ($E_C$) of BNT [20].The $E_C$ values are 4.69, 3.54, and 4.99 kV/mm for the compositions of $x$ = 0.02, 0.04, and 0.05, respectively (Fig. 4(b)). The values are significantly lower compared to pristine BNT, which has an $E_C$ of 7.3 kV/mm. The reduced $E_C$ can promote the domain switching during the poling process, and thus benefit the piezoelectric performance.

The bipolar $S(E)$ curves of all the investigated samples show an archetypal butterfly shape (Fig. 4(c)), which indicate the FE nature of the piezoelectric ceramics as well. Fig. 4(d) illustrates the total strain of the bipolar wave, defined as the absolute difference between its maximum and minimum strain values. The total strain increases non-monotonically with $x$, peaking at 0.195 % for the MPB composition of $x$ = 0.04 [34].

The thermal stability of polarization and strain-field behavior was evaluated by conducting temperature-dependent ferroelectric measurements on the 0.96BNT-0.04BSN sample. At 50 °C, the $P(E)$ loop is nearly saturated, demonstrating a characteristic ferroelectric behavior (Fig. 5(a)). However, when temperature reaches and exceeds 100 °C, the

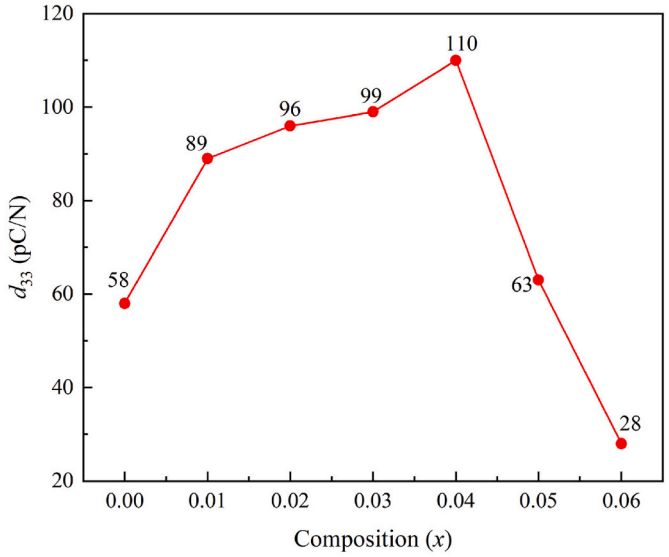


**Fig. 6.** The small-signal piezoelectric coefficient ($d_{33}$) as a function of BSN composition of (1-$x$)BNT-$x$BSN ceramics.

$P(E)$ loops become constricted. Both $E_C$ and $P_r$ drop sharply, suggesting an incipient presence of the anti-ferroelectric (AFE) order. With a further increase in temperature, the loops continuously become slimmer and more inclined, while $P_S$, $P_r$ and $E_C$ are further reduced (Fig. 5(c)). Fig. 5 (b) illustrates the bipolar $S(E)$ curves. The $S(E)$ curve displays a characteristic butterfly shape at 50 °C. As the temperature rises, the curve begins to change shape. The sudden increase in maximum strain, coupled with the near disappearance of negative strain around 150 °C, indicates a transition from the FE to AFE phase.

Fig. 5(d) illustrates that $S_{max}$ rises from 50 °C to 125 °C before declining, peaking at 125 °C, indicating a phase transition between 50 °C and 125 °C. The observed phenomenon can be explained by the dominance of the FE phase below 100 °C, resulting in minimal contribution of the FE-to-AFE transition to the strain. The AFE phase of BNT-BSN predominates when the temperature surpasses 100 °C, significantly contributing to the strain through the FE-to-AFE phase transition. This phenomenon has also been observed in various other BNT-based lead-free ceramics [23,35].

The small-signal piezoelectric coefficient ($d_{33}$) of all ceramics is shown in Fig. 6. Similar to the change of total strain, the $d_{33}$ is also enhanced non-monotonously with increasing $x$. The substitution of BSN significantly improves the piezoelectric coefficient. A maximum $d_{33}$ value of 110 pC/N has been observed in the MPB composition of 0.96BNT-0.04BSN, which is almost twice of the pristine BNT. The piezoelectric coefficient of 0.96BNT-0.04BSN ceramics surpasses many other BNT-based lead-free systems, such as 0.9625BNT-0.0375BZT ($d_{33}$ = 92 pC/N) and 0.93BNT-0.07BMN ($d_{33}$ = 94 pC/N), and is comparable to 0.94BNT-0.06$BaTiO_3$ ($d_{33}$ = 155 pC/N) [19,22,23,36]. The enhanced piezoelectric properties can be ascribed to the reduced $E_C$, facilitating the complete poling of ceramics during the process. Furthermore, the improved piezoelectric properties might be associated with the reduced depolarization temperature ($T_d$), which decreases from approximately 200 °C in pristine BNT to around 130 °C in 0.96BNT-0.04BSN, as will be elaborated in the subsequent section. A similar correlation between the piezoelectric coefficient and $T_d$ has been noted in conventional (1-$x$) BNT-$x$$BaTiO_3$ ceramics [37]. The loss of macro-ordering and reversion to a disordered micro-domain texture at $T_d$ indicates the stability of ferroelectric domains [38]. The decreased $T_d$ suggests that the introduction of BSN makes the ferroelectric domains less stable. Consequently, reorienting the 90 °C domains is facilitated. Therefore, enhanced piezoelectric properties were observed in the present (1-$x$) BNT-$x$BSN ceramics.

Since (1-$x$)BNT-$x$BSN ceramics exhibit favorable piezoelectric coefficients, the $T_C$ is another important factor for practical applications. To analyze the phase transition and determine the actual $T_C$, the temperature-dependent dielectric constant ($\varepsilon_r$) and loss (tan$\delta$) of (1-$x$) BNT-$x$BSN ceramics ($x$ = 0.02, 0.04, and 0.05) were measured across various frequencies from room temperature to 600 °C (Fig. 7(a–c)). All ceramics displayed two dielectric anomalies, indicating the FE-to-AFE phase transition temperatures, $T_d$ and $T_m$. Notably, a relaxor characteristic as a function of frequency at low temperature (<200 °C) has been observed for all investigated compounds, which could be ascribed to the structural disorder and compositional fluctuations. This effect has similarly been noted in other lead-free ceramics based on BNT [16,17]. The evolution of $T_m$ and $T_d$ derived from the dielectric spectroscopies are shown in Fig. 7(d). As can be seen, both $T_m$ and $T_d$ show decrease

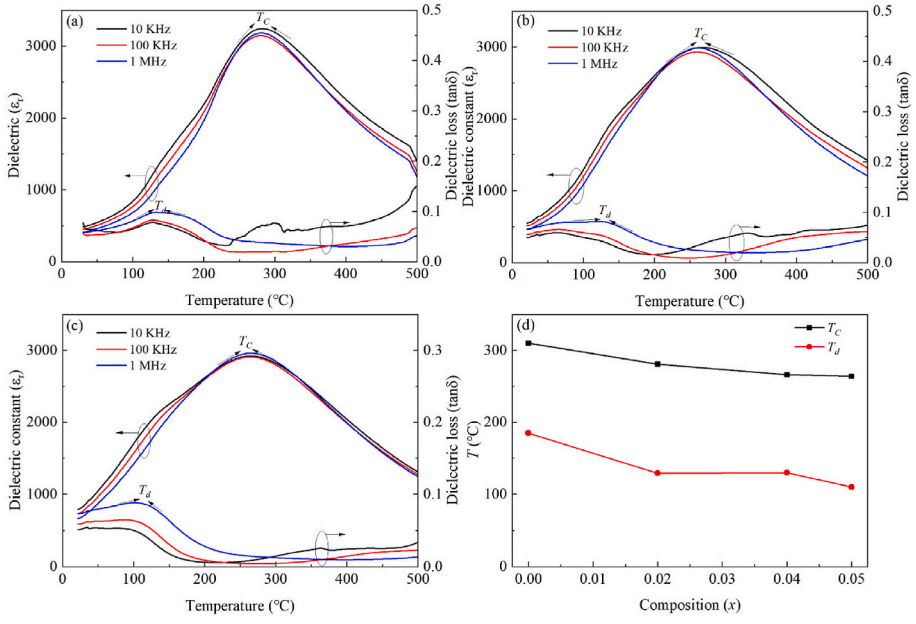


**Fig. 7.** The temperature dependence of dielectric constant ($\varepsilon_r$) and dielectric loss (tan$\delta$) of the (a) $x$ = 0.02, (b) $x$ = 0.04, and (c) $x$ = 0.05 ceramics, (d) $T_C$ and $T_d$ as function of composition $x$.

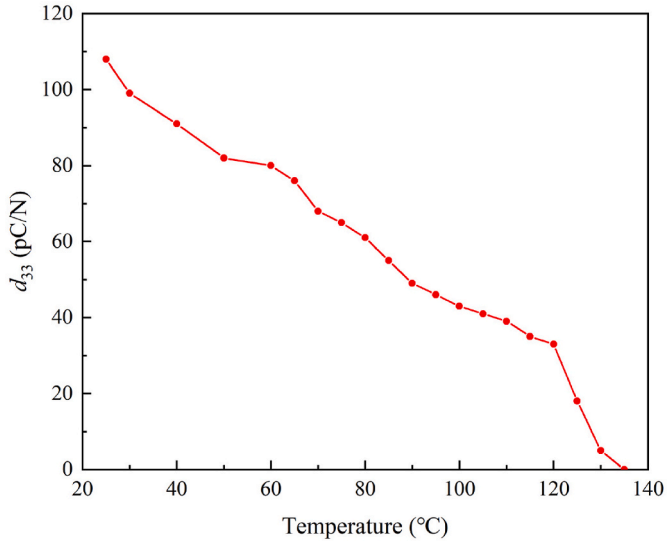


**Fig. 8.** Temperature dependence of small-signal $d_{33}$ of 0.96BNT-0.04BSN as function of annealing temperatures.

tendency with the increasing BSN content. The $T_m$ and $T_d$ values of the MPB composition 0.96BNT-0.04BSN are 266 and 130 °C, respectively.

Fig. 8 shows the effect of thermal depoling on the piezoelectric properties of 0.96BNT-0.04BSN ceramics with the optimal $d_{33}$ value at room temperature. As can be seen, the small-signal $d_{33}$ value of 0.96BNT-0.04BSN steadily decreases with increasing temperature. However, when the annealing temperature is approaching the $T_d$, the $d_{33}$ value decreases rapidly, and tends to zero, which corresponds to the FE-to-AFE phase transition. The result agrees well with the above mentioned temperature dependence $P(E)$ and $S(E)$ measurements, as well as the dielectric spectroscopy of the 0.96BNT-0.04BSN ceramics.

## 4. Conclusions

In summary, a novel lead-free piezoelectric system, $(1\text{-}x)Bi_{0.5}Na_{0.5}TiO_3\text{-}xBa(Sc_{0.5}Nb_{0.5})O_3$ ($0.00 \leq x \leq 0.06$), was developed and synthesized via the conventional solid solution method. All compositions display a perovskite structure, with the addition of BSN to BNT ceramics causing a phase transition from rhombohedral *R*3*c* to tetragonal *P*4*bm*. The incorporation of BSN effectively reduces the $E_C$ of pure BNT and enhances its piezoelectric properties. Composition for 0.96BNT-0.04BSN shows an enhanced piezoelectric coefficient of $d_{33} = 110$ pC/N, which is much higher than that of the pristine BNT. In addition, the 0.96BNT-0.04BSN compound also exhibit a moderate high $T_m$ of 266 °C. This study reaffirms that high piezoelectric performance is achievable in lead-free BNT-Ba*Me*$O_3$ systems.

## CRediT authorship contribution statement

**Weihao Li:** Writing – review & editing, Writing – original draft, Software, Formal analysis, Data curation. **Zhao Pan:** Writing – review & editing, Supervision, Project administration, Methodology, Funding acquisition, Conceptualization. **Mengqi Ye:** Writing – review & editing, Formal analysis, Data curation. **Jin Liu:** Writing – review & editing, Data curation. **Maocai Pi:** Writing – review & editing, Data curation. **Jie Zhang:** Writing – review & editing, Data curation. **Xubin Ye:** Writing – review & editing, Data curation. **Xiao Wang:** Data curation. **Nianpeng Lu:** Data curation. **Laijun Liu:** Writing – review & editing, Formal analysis, Data curation. **Enxiu Wu:** Writing – review & editing, Supervision, Funding acquisition. **Youwen Long:** Writing – review & editing, Supervision, Funding acquisition.

## Declaration of competing interest

The authors declare no competing financial interests.

## Acknowledgements

This work was supported by the National Key R&D Program of China (Grant No. 2021YFA1400300), the National Natural Science Foundation of China (22271309, 62204170, 12304268, 11934017, 11921004, and 12261131499), the Beijing Natural Science Foundation (Grant No. Z200007), and the Chinese Academy of Sciences (Grant No. XDB33000000).

## References

[1] G.H. Haertling, Ferroelectric ceramics: history and technology, J. Am. Ceram. Soc. 82 (1999) 797–818.
[2] D.A. Hall, Review nonlinearity in piezoelectric ceramics, J. Mater. Sci. 36 (2001) 4575–4601.
[3] S. Trolier-McKinstry, S. J. Zhang, A. J. Bell, X. L. Tan, High-performance piezoelectric crystals, ceramics, and films: D.R. Clarke (Ed.) Annu. Rev. Mater. Res., Vol 482018, pp. 191-217.
[4] P.K. Panda, B. Sahoo, PZT to lead free piezo ceramics: a Review, Ferroelectrics 474 (2015) 128–143.
[5] D.Q. Xiao, Environmentally conscious ferroelectrics research present and prospect, Ferroelectrics 231 (1999) 721–729.
[6] J. Rödel, W. Jo, K.T.P. Seifert, E.M. Anton, T. Granzow, D. Damjanovic, Perspective on the development of lead-free piezoceramics, J. Am. Ceram. Soc. 92 (2009) 1153–1177.
[7] M.H. Lee, D.J. Kim, J.S. Park, S.W. Kim, T.K. Song, M.H. Kim, W.J. Kim, D. Do, I. K. Jeong, High-performance lead-free piezoceramics with high curie temperatures, Adv. Mater. 27 (2015) 6976–6982.
[8] T. Takenaka, K. Maruyama, K. Sakata, $(Bi_{1/2}Na_{1/2})TiO_3$-$BaTiO_3$ system for lead-free piezoelectric ceramics, Jpn. J. Appl. Phys. 30 (1991) 2236.
[9] T. Yu, K.W. Kwok, H.L.W. Chan, The synthesis of lead-free ferroelectric $Bi_{0.5}Na_{0.5}TiO_3$-$Bi_{0.5}K_{0.5}TiO_3$ thin films by sol-gel method, Mater. Lett. 61 (2007) 2117–2120.
[10] A. Kounga, S.-T. Zhang, W. Jo, T. Granzow, J. Rodel, Morphotropic phase boundary in $(1\text{-}x)Bi_{0.5}Na_{0.5}TiO_3$-$xK_{0.5}Na_{0.5}NbO_3$ lead-free piezoceramics, Appl. Phys. Lett. 92 (2008) 222902, 222902.
[11] J. Jiang, X.J. Meng, L. Li, J. Zhang, S. Guo, J. Wang, X.H. Hao, H.G. Zhu, S. T. Zhang, Enhanced energy storage properties of lead-free $NaNbO_3$-based ceramics via A/B-site substitution, Chem. Eng. J. 422 (2021).
[12] M.X. Zhou, R.H. Liang, Z.Y. Zhou, X.L. Dong, Superior energy storage properties and excellent stability of novel $NaNbO_3$-based lead-free ceramics with A-site vacancy obtained via a $Bi_2O_3$ substitution strategy, J. Mater. Chem. A 6 (2018) 17896–17904.
[13] Y. Li, W. Chen, J. Zhou, Q. Xu, H. Sun, R. Xu, Dielectric and piezoelecrtic properties of lead-free $(Na_{0.5}Bi_{0.5})TiO_3$-$NaNbO_3$ ceramics, Mater. Sci. Eng., B 112 (2004) 5–9.
[14] R. Cheng, Z. Xu, R. Chu, J. Hao, J. Du, W. Ji, G. Li, Large piezoelectric effect in $Bi_{1/2}Na_{1/2}TiO_3$-based lead-free piezoceramics, Ceram. Int. 41 (2015) 8119–8127.
[15] M. Ozgul, A. Kucuk, $B_2O_3$ doping in $0.94(Bi_{0.5}Na_{0.5})TiO_3$-$0.06BaTiO_3$ lead-free piezoelectric ceramics, Ceram. Int. 42 (2016) 19119–19123.
[16] X. Li, B. Zhang, X. Cao, B. Peng, K. Ren, Large strain response in $(Bi_{0.5}Na_{0.5})TiO_3$-$6BaTiO_3$-based lead-free ceramics at high temperature, Ceram. Int. 48 (2022) 9051–9058.
[17] H. He, X. Lu, E. Hanc, C. Chen, H. Zhang, L. Lu, Advances in lead-free pyroelectric materials: a comprehensive review, J. Mater. Chem. C 8 (2020) 1494–1516.
[18] H. Ji, D. Wang, W. Bao, Z. Lu, G. Wang, H. Yang, A. Mostaed, L. Li, A. Feteira, S. Sun, F. Xu, D. Li, C.-J. Ma, S.-Y. Liu, I.M. Reaney, Ultrahigh energy density in short-range tilted NBT-based lead-free multilayer ceramic capacitors by nanodomain percolation, Energy Storage Mater. 38 (2021) 113–120.
[19] C. Xu, D. Lin, K.W. Kwok, Structure, electrical properties and depolarization temperature of $(Bi_{0.5}Na_{0.5})TiO_3$-$BaTiO_3$ lead-free piezoelectric ceramics, Solid State Sci. 10 (2008) 934–940.
[20] J. Yin, H. Tao, G. Liu, J.G. Wu, Domain-scale imaging to dispel the clouds over the thermal depolarization of $Bi_{0.5}Na_{0.5}TiO_3$-based relaxor ferroelectrics, J. Am. Ceram. Soc. 103 (2020) 1881–1890.
[21] A. Sasaki, T. Chiba, Y. Mamiya, E. Otsuki, Dielectric and piezoelectric properties of $(Bi_{0.5}Na_{0.5})TiO_3$-$(Bi_{0.5}K_{0.5})TiO_3$ systems, Jpn. J. Appl. Phys. 38 (1999) 5564.
[22] S.-T. Zhang, F. Yan, B. Yang, Morphotropic phase boundary and electrical properties in $(1\text{-}x)Bi_{0.5}Na_{0.5}TiO_3$-$xBi(Zn_{0.5}Ti_{0.5})O_3$ lead-free piezoceramics, J. Appl. Phys. 107 (2010) 114110, 114110.
[23] Q. Wang, J. Chen, L. Fan, L. Liu, L. Fang, X. Xing, J.L. Jones, Preparation and electric properties of $Bi_{0.5}Na_{0.5}TiO_3$-$Bi(Mg_{0.5}Ti_{0.5})O_3$ lead-free piezoceramics, J. Am. Ceram. Soc. 96 (2012) 1171–1175.
[24] X.F. Zhou, C. Jiang, H. Luo, C. Chen, K.C. Zhou, D. Zhang, Enhanced piezoresponse and electric field induced relaxor-ferroelectric phase transition in NBT-0.06BT ceramic prepared from hydrothermally synthesized nanoparticles, Ceram. Int. 42 (2016) 18631–18640.
[25] W. Bai, Y. Bian, J. Hao, B. Shen, J. Zhai, S. Zhang, The composition and temperature-dependent structure evolution and large strain response in $(1\text{-}x)$

$(Bi_{0.5}Na_{0.5})TiO_3$-$x$Ba$(Al_{0.5}Ta_{0.5})O_3$ ceramics, J. Am. Ceram. Soc. 96 (2012) 246–252.
[26] B. Parija, T. Badapanda, S. Panigrahi, Morphotropic phase boundary in BNT-BZT solid solution: a study by Raman spectroscopy and electromechanical parameters, J. Ceram. Process. Res. 16 (2015) 565–571.
[27] Z. Pan, M. An, J. Chen, L. Fan, L. Liu, L. Fang, X. Xing, Preparation and electrical properties of the new lead-free (1-$x$)$(Bi_{0.5}Na_{0.5})TiO_3$-$x$Ba$(Ni_{1/3}Nb_{2/3})O_3$ piezoelectric ceramics, J. Ceram. Soc. Jpn. 123 (2015) 1038–1042.
[28] Y. Hiruma, H. Nagata, T. Takenaka, Formation of morphotropic phase boundary and electrical properties of $(Bi_{1/2}Na_{1/2})TiO_3$-Ba$(Al_{1/2}Nb_{1/2})O_3$ solid solution ceramics, Jpn. J. Appl. Phys. 48 (2009).
[29] H. Wang, R. Zuo, Y. Liu, J. Fu, Densification behavior, microstructure, and electrical properties of sol-gel-derived niobium-doped $(Bi_{0.5}Na_{0.5})$0.94Ba0.06$TiO_3$ ceramics, J. Mater. Sci. 45 (2010) 3677–3682.
[30] N.J. Donnelly, T.R. Shrout, C.A. Randall, Addition of a Sr, K, Nb (SKN) combination to PZT(53/47) for high strain applications, J. Am. Ceram. Soc. 90 (2007) 490–495.
[31] R.E. Eitel, C.A. Randall, T.R. Shrout, P.W. Rehrig, W. Hackenberger, S.E. Park, New high temperature morphotropic phase boundary piezoelectrics based on Bi(Me)$O_3$-$PbTiO_3$ ceramics, Jpn. J. Appl. Phys. 40 (2001) 5999–6002.
[32] R.D. Shannon, Revised effective ionic radii and systematic studies of interatomie distances in halides and chaleogenides, Acta Crystallogr. A32 (1976) 751–767.
[33] B.H. Toby, R.B. Von Dreele, *GSAS-II*: the genesis of a modern open-source all purpose crystallography software package, J. Appl. Crystallogr. 46 (2013) 544–549.
[34] Z. Pan, J. Chen, L. Fan, Y. Rong, S. Zheng, L. Liu, L. Fang, X. Xing, Enhanced high-temperature piezoelectric properties of traditional Pb(Zr,Ti)$O_3$ ceramics by a small amount substitution of $KNbO_3$, Mater. Res. Express 1 (2014) 046301.
[35] Q. Wang, J. Chen, L. Fan, H. Song, W. Gao, Y. Rong, L. Liu, L. Fang, X. Xing, Preparation and electric properties of $Bi_{0.5}Na_{0.5}TiO_3$-Bi$(Al_{0.5}Ga_{0.5})O_3$ lead-free piezoceramics, J. Am. Ceram. Soc. 96 (2013) 3793–3797.
[36] C.R. Zhou, X.Y. Liu, Dielectric and piezoelectric properties of bismuth-containing complex perovskite solid solution of $Bi_{1/2}Na_{1/2}TiO_3$-Bi$(Mg_{2/3}Nb_{1/3})O_3$, J. Mater. Sci. 43 (2008) 1016–1019.
[37] B.J. Chu, D. Chen, G. Li, Q. Yin, Electrical properties of $Na_{1/2}Bi_{1/2}TiO_3$-$BaTiO_3$ ceramics, J. Eur. Ceram. Soc. 22 (2002) 2115–2121.
[38] X. Yao, Z.L. Chen, L.E. Cross, Polarization and depolarization behavior of hot pressed lead lanthanum zirconate titanate ceramics, J. Appl. Phys. 54 (1983) 3399–3403.